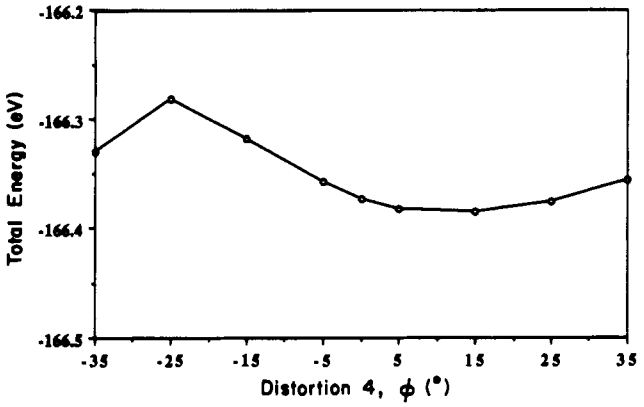


**Figure 11.** Total energy plot for distortion 4.

the COOP curve for distortion 1 (Figure 8 above).

Finally, we consider distortion 4, a transition from distortion 1 to distortion 3. Figure 11 shows a plot of the total energy for distortion 4 in which $\theta$ is kept constant at 35° while $\phi$ is varied between −35 and +35° (see **4**). The energy barrier for this rotation is small (~0.1 eV); however, the energy minimum is substantially offset from 35°. As the dicarbide unit rotates beyond $\phi = 0°$, an unfavorable overlap between the $2\sigma_u$ orbitals on the paired dicarbides arises. Hence, the minimum in energy near $\phi = 15°$ is a result of the fine tuning of interactions between C and Ca, and the interaction between dicarbide units. Interestingly, since the point at $\phi = 0°$ is not a minimum, the distortion of a single unit initates the distortion of its neighbors. Thus, if one dicarbide unit is provided with enough energy to rotate, then the distortion can, to some extent, propagate through the solid.

### Concluding Remarks

As we have seen, the original structure of $CaC_2$ is indeed the most stable one, at least with our approximate molecular orbital calculations. However, the barrier for rotation of the $C_2$ dimer away from the *c*-axis is extremely small; significant population of rotated geometries is possible at room temperature. Therefore, at higher temperatures we might expect a very different structure, and indeed, at least four metastable phases of $CaC_2$ have been reported.[12] From our analyses of these distortions, we propose a fluxional model in which the dicarbide unit, while preferring a time-averaged alignment with the *c*-axis, spends some part of its time distorted in the direction of a face of its coordination octahedron and the least amount of its time distorted toward an edge. A similar model has been proposed for NaCN at room temperature in a single-crystal neutron diffraction study.[13] Such a study on $CaC_2$ would resolve this issue but awaits successful growth of sizeable pure crystals.

### Appendix

An extended Hückel tight-binding approach was employed in all of the calculations. The atomic parameters used were taken from previous work[6a,14] and are tabulated in Table I. A set of 125 k-points was used for calculations of average properties. The band structures were calculated at 6 k-points along each line between special points in the Brillouin zone.

**Acknowledgment.** This work was supported by the National Science Foundation through Research Grants CHE-8912070 and DMR-8818558.

**Registry No.** $CaC_2$, 75-20-7.

(12) (a) Bredig, M. A. *Z. Anorg. Allg. Chem.* **1961**, *310*, 338. (b) Vannerberg, N.-G. *Acta Chem. Scand.* **1962**, *15*, 769. (c) Vannerberg, N.-G. *Acta Chem. Scand.* **1961**, *16*, 1212.
(13) Rowe, R. M.; Hinks, D. G.; Price, D. L.; Susman, S.; Rush, J. J. *J. Chem. Phys.* **1973**, *58*, 2039.
(14) Zheng, C.; Hoffmann, R. *J. Am. Chem. Soc.* **1986**, *108*, 3078.

Contribution from the Department of Synthetic Chemistry, Faculty of Engineering, Kyoto University, Kyoto 606, Japan

# Electronic Structures of Dative Metal–Metal Bonds: Ab Initio Molecular Orbital Calculations of $(OC)_5Os-M(CO)_5$ (M = W, Cr) in Comparison with $(OC)_5M-M(CO)_5$ (M = Re, Mn)

H. Nakatsuji,* M. Hada, and A. Kawashima

*Received November 8, 1991*

The nature of the metal–metal bonds in the binuclear complexes $(OC)_5Os-M(CO)_5$ (M = W, Cr) is studied by ab initio MO calculations and compared with that of the covalent metal–metal bonds in $(OC)_5M-M(CO)_5$ (M = Re, Mn). We confirm that the former complexes have a dative metal–metal bond, as suggested experimentally. The $Os(CO)_5$ fragment, which has an 18-electron configuration, acts as an electron donor to the $M(CO)_5$ (M = W, Cr) fragments, which have 16-electron configurations, to form stable binuclear complexes. The highest occupied $\sigma$-orbital of $Os(CO)_5$ and the lowest unoccupied $\sigma$-orbital of $M(CO)_5$ (M = W, Cr) interact and form the metal–metal dative $\sigma$-bonding orbital. The electron transfer occurs not only around the two metals, but also within each fragment, including CO ligands. The calculated bond formation energies are 20.9 and 7.7 kcal/mol for $(OC)_5Os-W(CO)_5$ and $(OC)_5Os-Cr(CO)_5$, respectively. They are smaller than those of the covalent complexes $(OC)_5M-M(CO)_5$ (M = Re, Mn), 54.0 kcal/mol for M = Re and 32.5 kcal/mol for M = Mn. However, the bond lengths and the force constants of the Os–W and Os–Cr bonds are comparable with those of the Re–Re and Mn–Mn bonds. The calculated distances are 3.04, 2.86, 2.98, and 2.86 Å and force constants are 1.08, 0.79, 1.53, and 0.66 mdyn/Å for Os–W, Os–Cr, Re–Re, and Mn–Mn, respectively. These values reasonably agree with the experimental values. The smallness of the bond formation energy in $(OC)_5Os-M(CO)_5$ (M = W, Cr) is mainly due to a large geometrical relaxation of the $Os(CO)_5$ fragment in the course of the dissociation. In $(OC)_5Os-M(CO)_5$, the HOMO is a metal–metal $\sigma$-bonding orbital for M = Cr, but metal–ligand $\pi$-bonding orbital for M = W. The metal–metal $\sigma$-bond is stronger in $(OC)_5Os-W(CO)_5$ than in $(OC)_5Os-Cr(CO)_5$, and different reactivities are expected for electrophiles.

### Introduction

The possibility that a neutral 18-electron transition-metal compound can act as a two-electron donor to the 16-electron transition-metal compound to form a dative metal–metal bond has been suggested for a long time. The first such report appears to be that of Hock and Mills for $Fe_2(\mu\text{-}CO)(CO)_5(C_4R_4)$.[1] However, two alternative electron-counting schemes are possible for this complex, so that this metal–metal bond can also be re-

(1) Hock, A. A.; Mills, O. S. *Acta Crystallogr.* **1961**, *14*, 139.

0020-1669/92/1331-1740$03.00/0 

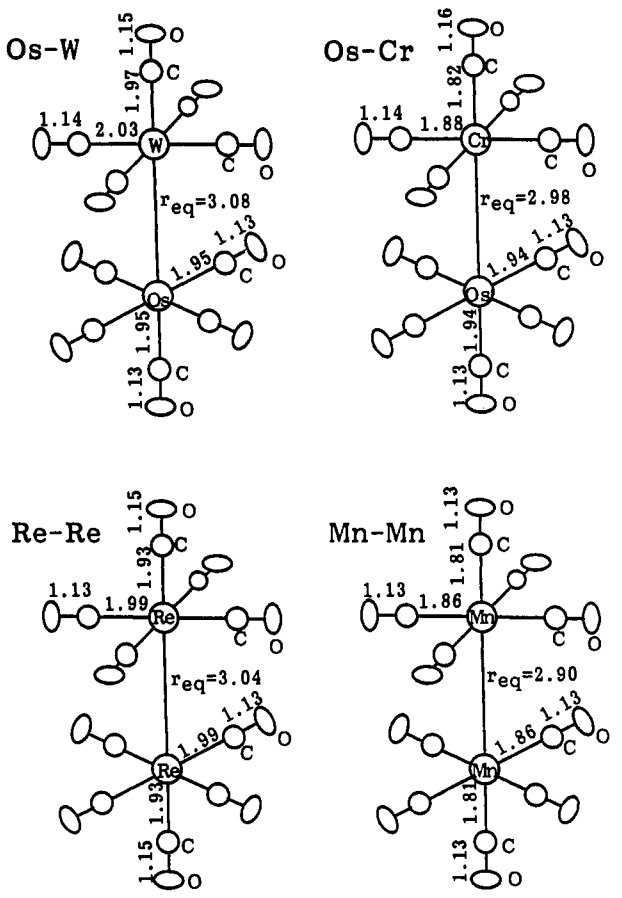


**Figure 1.** Geometries of the complexes used in the present calculations. These are the experimental values taken from refs 5 and 14.

garded as a nondative, covalent bond. In most complexes where dative bonds may be present, they may also be regarded as being supported by bridging ligands or nondative metal–metal bonds in a cluster framework.[2] In anionic complexes, for example, $(OC)_5M'$–$M(CO)_5^-$ (M′ = Mn, Re; M = Cr, Mo, W)[3] and $H(CO)_4Fe$–$M(CO)_5^-$ (M = Cr, W),[4] there is also an ambiguity in the electron-counting for the anionic charge.

Recently, Davis et al. reported the synthesis of $(Me_3P)(OC)_4Os$–$M(CO)_5$ (M = Cr, W),[5] which are neutral, unbridged binuclear complexes. They suggested that the $Os(PMe_3)(CO)_4$ fragment acts as a donor ligand to the second metal atom and forms a drive metal–metal bond. They also reported the $(OC)_5Os$–$Cr(CO)_5$ complex, but it was unstable in solution at room temperature.

Hoffmann et al. reported a theoretical study on the electronic structure of $M(CO)_n$ ($n$ = 3–5) fragments and their bonding capabilities with the second fragments.[6] They also studied the bridged and unbridged $M_2(CO)_{10}$ complexes.[7] Barr et al. studied theoretically the bonding nature in the complexes $Cr(\mu\text{-}CO)_2(CO)(\eta\text{-}C_6H_6)Rh(CO)(\eta\text{-}C_5Me_5)$ and $Co(\mu\text{-}CO)_2(\eta\text{-}C_5H_5)Rh(PH_3)(\eta\text{-}C_5H_5)$. Though the presence of the dative metal–metal bond was indicated, they concluded that it is weak and chiefly supported by the bridging carbonyls.[8]

**Table I.** Properties of the Metal–Metal Bonds in the Binuclear Complexes $(OC)_5Os$–$M(CO)_5$ (M = W, Cr) and $(OC)_5M$–$M(CO)_5$ (M = Re, Mn)

| property | | complex | | | |
|---|---|---|---|---|---|
| | | OsW | $Re_2$ | OsCr | $Mn_2$ |
| M–M bond length, Å | calcd | 3.04 | 2.98 | 2.86 | 2.86 |
| | exptl | 3.08 | 3.04 | 2.98 | 2.90 |
| force constant, mdyn/Å | calcd | 1.08 | 1.53 | 0.79 | 0.66 |
| | exptl | | 0.82 | | 0.59 |
| rotational barrier, kcal/mol | calcd | 4.45 | 4.57 | 5.91 | 5.52 |

**Table II.** Metal–Metal Bond Formation Energy from Frozen-Geometry Fragments and Geometry-Optimized Fragments (kcal/mol)

| geometry of the fragments | Os–W | Re–Re | Os–Cr | Mn–Mn |
|---|---|---|---|---|
| frozen[a] | 57.1 | 69.4 | 44.2 | 49.9 |
| optimized | 20.9 | 54.0 | 7.7 | 32.5 |
| exptl | | 51 | | 22 |

[a] Geometries of the fragments are fixed to those in the binuclear complexes.

We have reported ab initio MO studies on the electronic structure and the bonding nature of the bridged Rh–Rh bond in dirhodium tetracarboxylate complexes[9] and on the nature of the metal–carbon and metal–silicone double bonds.[10]

In this paper, we report ab initio MO studies for $(OC)_5Os$–$M(CO)_5$ (M = W, Cr) and $(OC)_5M$–$M(CO)_5$ (M = Re, Mn). We confirm that the former complexes have a dative metal–metal bond in which the osmium fragment has an 18-electron configuration and acts a donor ligand to the $M(CO)_5$ (M = W, Cr) fragments in which M has a 16-electron configuration. The latter has a typical covalent M–M bond in which the metal fragment has a 17-electron configuration. We also study the nature of the dative metal–metal bonds in comparison with the covalent ones. Geometries of the isolated fragments of each complex are also examined for calculating the dissociation energy.

## Calculation Details

All calculations are based on the ab initio RHF–SCF MO theory. The program used in the present calculations is HONDO7.[11] The basis sets for the Os, W, and Re atoms are (3s3p3d)/[3s2p2d], those for Mn and Cr are (3s2p5d)/[3s2p2d], and the core electrons are replaced by the effective core potentials reported by Hay and Wadt.[12] For C and O, we used the (33/3) sets reported by Huzinaga et al.[13] The internuclear distances in $(OC)_5Os$–$M(CO)_5$ (M = W, Cr) are taken from the X-ray data for the similar complexes $(Me_3P)(CO)_4Os$–$M(CO)_5$ (M = W, Cr).[5] The distances in $(OC)_5M$–$M(CO)_5$ (M = Re, Mn) are also taken from the experimental data.[14] Figure 1 shows the distances used in the present calculations. It also shows the equilibrium M–M distances observed experimentally. All of the C–M–C angles are fixed at 90°. In calculating the potential curves, force constants, and equilibrium distances of the metal–metal bonds, the geometries of the ligands are fixed throughout.

We also investigate the geometry of the isolated fragments $M(CO)_5$ (M = Os, W, Cr, Re, Mn). The internuclear distances are taken equal to those in the binuclear complexes. We examine the stability of trigonal bipyramid and normal and distorted square pyramids.


(2) (a) Gelmini, L.; Stephan, D. W. *Organometallics* **1988**, *7*, 849. (b) John, G. R.; Johnson, B. F. G.; Lewis, J. *J. Organomet. Chem.* **1979**, *181*, 143. (c) Bruce, M. I.; Williams, M. L. *J. Organomet. Chem.* **1985**, *282*, C11.
(3) Anders, U.; Graham, W. A. G. *J. Am. Chem. Soc.* **1967**, *89*, 539.
(4) Arndt, L. W.; Darensbourg, M. Y.; Delord, T.; Bancroft, B. T. *J. Am. Chem. Soc.* **1986**, *108*, 2617.
(5) Davis, H. B.; Einstein, F. W. B.; Glavina, P. G.; Jones, T.; Pomeroy, R. K.; Rushman, P. *Organometallics* **1989**, *8*, 1030.
(6) Elian, M.; Hoffmann, R. *Inorg. Chem.* **1975**, *14*, 1058.
(7) Shaik, S.; Hoffmann, R.; Fisel, C. R.; Summerville, R. H. *J. Am. Chem. Soc.* **1980**, *102*, 4555.
(8) Barr, R. D.; Marder, T. B.; Orpen, A. G.; Williams, I. D. *J. Chem. Soc., Chem. Commun.* **1984**, 112.
(9) (a) Nakatsuji, H.; Onishi, Y.; Ushio, J.; Yonezawa, T. *J. Inorg. Chem.* **1983**, *22*, 1623. (b) Nakatsuji, H.; Ushio, J.; Kanda, K.; Onishi, Y.; Kawamura, T.; Yonezawa, T. *Chem. Phys. Lett.* **1981**, *79*, 299.
(10) (a) Nakatsuji, H.; Ushio, J.; Han, S.; Yonezawa, T. *J. Am. Chem. Soc.* **1983**, *105*, 426. (b) Ushio, J.; Nakatsuji, H.; Yonezawa, T. *J. Am. Chem. Soc.* **1984**, *106*, 5892. (c) Nakatsuji, H.; Ushio, J.; Yonezawa, T. *J. Organomet. Chem.* **1983**, *258*, C1.
(11) Dupuis, M. S.; Watts, J. D.; Villar, H. O.; Hurst, G. J. B. *HONDO*, version 7; Scientific And Engineering Computations Dept. 48B, IBM Corp.: New York, 12401; 1978.
(12) Hay, P. J.; Wadt, W. R. *J. Chem. Phys.* **1985**, *82*, 270.
(13) *Gaussian Basis Sets for Molecular Calculations*; Huzinaga, S., Ed.; Physical Data 16; Elsevier Science Publishing Co. Inc.: New York, 1984.
(14) Churchill, M. R.; Amoh, K. N.; Wasserman, H. J. *Inorg. Chem.* **1981**, *20*, 1609.

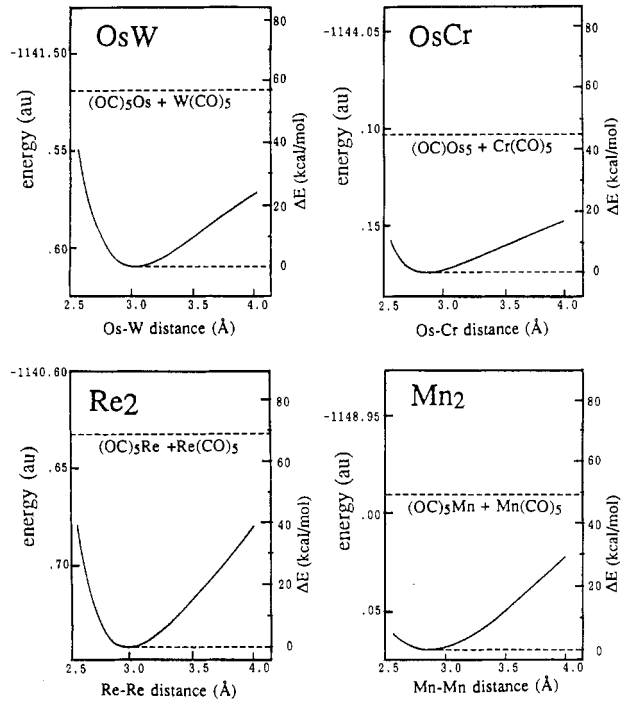


**Figure 2.** Potential curves for the stretching of the metal–metal bond in the binuclear complexes; $(OC)_5Os$–$M(CO)_5$ (M = Cr, W) and $(OC)_5M$–$M'(CO)_5$ (M = Mn, Re) with the geometries of the fragments fixed. Broken lines indicate the total energy of the two fragments at the dissociation limit.

The $(OC)_5M$–$M'(CO)_5$ complex will be indicated as the M–M′ complex for short in the following text.

## Results and Discussions

**A. Structures and Stabilities.** Figure 2 shows the potential energy curves for the stretching of the M–M bond of the binuclear complexes with fixing the geometries of the ligands. The broken lines indicate the total energy at the dissociation limit; the energy of the two fixed-geometry fragments. We see from this figure that the dative Os–W and Os–Cr bonds are as stable as the covalent Re–Re and Mn–Mn bonds. The bond lengths and force constants calculated from these potential curves are summarized in Table I. The equilibrium bond length is calculated to be 3.04 and 2.86 Å for the Os–W and Os–Cr complexes, respectively. They agree well with the experimental values 3.08 and 2.98 Å, respectively, of the similar complexes $(Me_3P)(CO)_4Os$–$M(CO)_5$ (M = W, Cr).[5] Usually, the Hartree–Fock theory tends to give larger M–M interactions than actually are, so that the calculated bond distances are smaller than the experimental ones.

All of the complexes are stable at the staggered form, and this form agrees with the results of the X-ray analyses.[5,14] The rotational barriers are 4–6 kcal/mol, as shown in Table I, and free rotations are expected at room temperature. In ethane, the rotational barrier of C–C is 2.9 kcal/mol.[15]

These results show that the dative metal–metal bonds are certainly as stable as the covalent metal–metal bonds. We next examine the bond formation energy of the metal–metal bonds. Table II shows two types of stabilization energy of the binuclear complexes. The upper value is the stabilization energy when the two fixed-geometry fragments form the binuclear complex $(OC)_5M$–$M'(CO)_5$, i.e., the bond energy calculated from Figure 1. The lower one is the stabilization energy relative to the two fragments whose geometries are optimized at the dissociation limit. The dative Os–W and Os–Cr bonds are less stable than the covalent Re–Re and Mn–Mn bonds, when the geometry relaxation during the dissociation process is taken into account. In particular, the stabilization energy of the Os–Cr complex becomes only 7.7 kcal/mol.

(15) Lowe, J. P. *Prog. Phys. Org. Chem.* **1968**, *6*, 1.

**Table III.** Relaxation Energies of the Fragments at the Dissociation Limit[a]

| property | fragment | | | | |
|---|---|---|---|---|---|
| | $Os(CO)_5$ | $W(CO)_5$ | $Cr(CO)_5$ | $Re(CO)_5$ | $Mn(CO)_5$ |
| structure[b] | tbp | sp 91° | sp 91° | sp 96° | sp 97° |
| relaxation energy, kcal/mol | 36.1 | 0.1 | 0.4 | 7.7 | 8.7 |

[a] Relative to the square-pyramid structure in the complex. [b] See Figure 3.

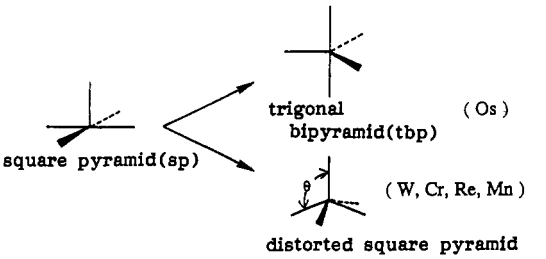


**Figure 3.** Two relaxation modes of the fragments at the dissociation limit considered in the present calculations.

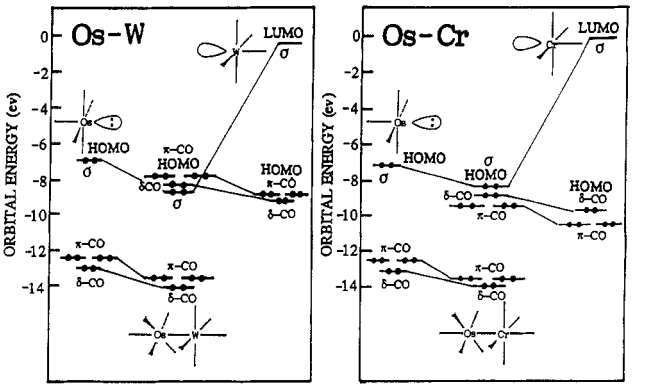


**Figure 4.** Orbital correlation diagrams for $(OC)_5Os$–$M(CO)_5$ (M = W, Cr) from $Os(CO)_5$ and $M(CO)_5$ (M = W, Cr).

Table III shows the relaxation energy of the $M(CO)_5$ fragments (M = Os, W, Cr, Mn, Re). We consider two types of geometry relaxations of the fragments, as shown in Figure 3. One is the relaxation to the trigonal-bipyramid (tbp) structure and the other to the distorted-square-pyramid (sp) structure in which the radial CO ligands are not coplanar. The metal–C and C–O distances are fixed throughout the calculations. Only $Os(CO)_5$ obtains the tbp structure at the dissociation limit, and the relaxation energy is as large as 36.1 kcal/mol. For the other fragments, the geometries are relaxed to the distorted sp structure and the relaxation energies range from 0.1 to 8.7 kcal/mol. Thus, the geometrical relaxation of the $Os(CO)_5$ fragment is largest and causes the smallness of the bonding energy of the dative Os–M (M = W, Cr) bonds relative to that of the covalent M–M (M = Mn, Re) bonds.

**B. Properties of the Metal–Metal Bonds.** The bond length, force constant, and rotational barrier of each complex are summarized in Table I. The structures of the fragments are fixed throughout the calculations. The metal–metal distances of the Re–Re and Mn–Mn complexes agree well with the experimental values.[14] Those of the Os–W and Os–Cr complexes also agree with those of similar complexes, $(Me_3P)(CO)_4Os$–$M(CO)_5$ (M = W, Cr).[5] The rotational barriers of the Os–W and Re–Re complexes are smaller than those of the Os–Cr and Mn–Mn complexes. This may be caused by the difference in the steric repulsions between the radial CO ligands of both sides, since the Os–W and Re–Re bonds are longer than Os–Cr and Mn–Mn bonds.

The force constants of the dative metal–metal bonds are almost equivalent to those of the covalent ones. This shows that the

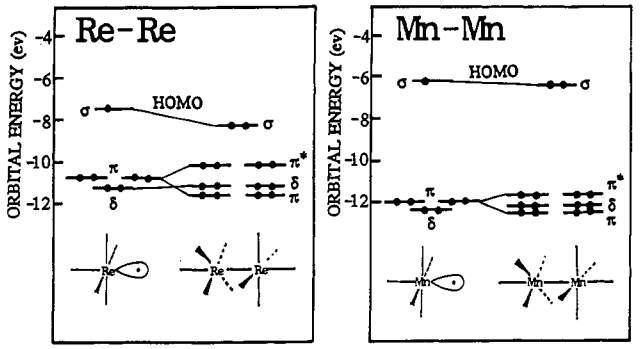


**Figure 5.** Orbital correlation diagrams for $(OC)_5M-M(CO)_5$ from $M(CO)_5$ (M = Mn, Re).

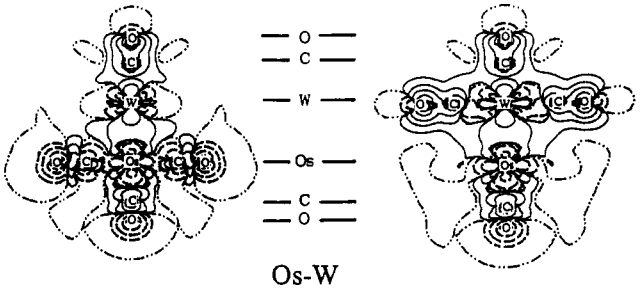


**Figure 6.** Contour maps of the electron density difference of $(OC)_5Os-W(CO)_5$. The map on the right-hand side is rotated 45° around the metal–metal bond, so that the radial CO ligands on the other side can be seen. The solid and broken lines indicate the increase in electron density and the decrease relative to those of the fragments. (See eq 1 for the definition of the electron density difference).

strength of the dative metal–metal bonds is comparable with that of the covalent ones at the equilibrium metal–metal distance. The present calculations overestimate the force constants of the Re–Re and Mn–Mn complexes, though this order of overestimation seems to be reasonable in the Hartree–Fock calculations.

**C. Orbital Nature of the Complexes.** Figure 4 shows the orbital correlation diagrams for the formation of the Os–W and Os–Cr complexes from the $Os(CO)_5$ and $M(CO)_5$ fragments. The highest occupied molecular orbital (HOMO) of $Os(CO)_5$ is the spd-hybrid $\sigma$-orbital extending outward. The lowest unoccupied MO (LUMO) of $W(CO)_5$ and $Cr(CO)_5$ are the $\sigma$-orbitals whose lobes extend outward. The lower three orbitals of all the fragments are the $\pi$- and $\delta$-orbitals which are mainly bonding between the metal and the CO ligands. The electron-pair transfer from the HOMO of $Os(CO)_5$ to the LUMO of $M(CO)_5$ (M = W, Cr) leads to the formation of the Os–M $\sigma$-bond of the binuclear complexes. This donation of the electron-pair of the $Os(CO)_5$ fragment to the $M(CO)_5$ (M = W, Cr) fragments is the origin of the dative metal–metal bond. There are no back-donating orbitals in these complexes. The $\sigma$-bonding orbital in the Os–Cr complex is less stable than that in the Os–W complex, so this orbital appears as the HOMO in the Os–Cr complex. This is why the bond formation energy of the Os–Cr complex shown in Table II is smaller than that of the Os–W complex. The other orbitals, $\delta$- and $\pi$-orbitals, essentially keep their nature in the complexes. However, we note that these metal–CO bond orbitals are stabilized in the donor fragments after the M–M bond formation but destabilized in the acceptor fragments. The reason will be explained below by using the electron density map.

Figure 5 shows the corresponding orbital correlation diagrams for the covalent complexes $(OC)_5M-M(CO)_5$ (M = Mn, Re). In the $M(CO)_5$ fragment, the spd hybrid $\sigma$-orbitals of the fragments are singly occupied and form the M–M $\sigma$-bonding orbital of the complexes. The other $\delta$- and $\pi$-orbitals do not contribute to the metal–metal bonds. Their energy levels scarcely change in the complex formation process in contrast to the cases of the dative Os–W and Os–Cr bonds.

**D. Contour Maps of Electron Density.** Figures 6 and 7 show the contour maps for the changes in the electron density due to

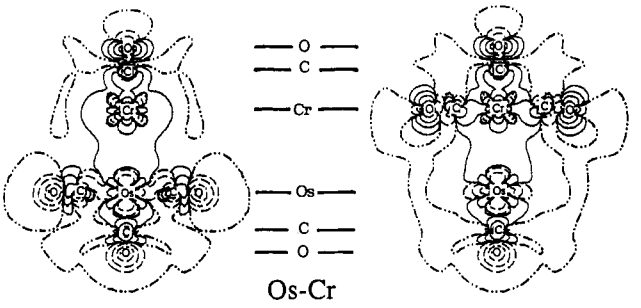


**Figure 7.** Contour maps of the electron density difference of $(OC)_5Os-Cr(CO)_5$. The map on the right-hand side is rotated 45° around the metal–metal bond, so that the radial CO ligands on the other side can be seen. The solid and broken lines indicate the increase in electron density and the decrease relative to those of the fragments. (See eq 1 for the definition of the electron density difference).

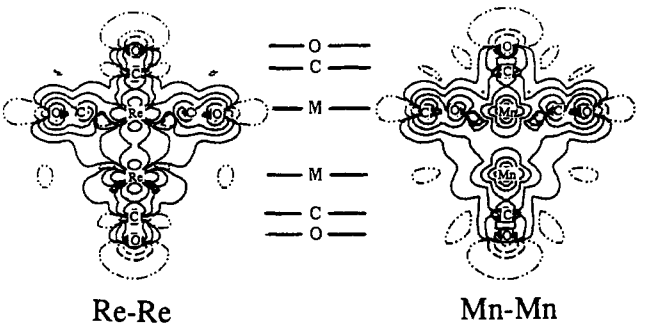


**Figure 8.** Contour map of the electron density difference of $(OC)_5M-M(CO)_5$ (M = Mn, Re). The solid and broken lines indicate the increase in electron density and the decrease relative to those of the fragments. (See eq 1 for the definition of the electron density difference).

the formations of the dative Os–W and Os–Cr bonds, respectively. Figure 8 shows the corresponding contour maps for the Re–Re and Mn–Mn complexes. The electron density difference is defined by

$$\Delta\rho = \rho[(OC)_5M-M'(CO)_5] - \rho[(OC)_5M] - \rho[M'(CO)_5] \quad (1)$$

The contour maps on the left-hand sides of Figures 6 and 7 are plotted on the plane which involves the radial CO's bonding with the Os atom. Those on the right-hand sides are for the plane of the radial CO's bonding with the W and Cr atoms. The solid line indicates an increase in the electron density, and the broken line, a decrease. These contour maps are drawn at the equilibrium metal–metal length. On around the Os–M axis, the electron density decreases around the Os atom and increases around the W and Cr atoms. Further, the electron transfer occurs not only around the metal atoms but also around the radial CO ligands.

The contour maps of the Re–Re and Mn–Mn complexes are shown in Figure 8. They are for the typical covalent metal–metal bonds. The electron transfer seems to occur from the oxygen lone pairs to the metal–metal and metal–ligand bonds.

The contour maps of the HOMO's and LUMO's of the Os–W and Os–Cr complexes are displayed in Figure 9. The HOMO of the Os–Cr complex is the metal–metal-bonding $\sigma$-orbital, but in the Os–W complex, the HOMO is a metal–CO-bonding orbital which has an antibonding nature between the two metal atoms. Figure 9 also depicts the Os–W $\sigma$-bonding MO, which is more stable than the Os–Cr $\sigma$-MO and therefore is not the HOMO. This result suggests that the reactivities of these two complexes, $(OC)_5Os-M(CO)_5$ (M = W, Cr), should be different for electrophiles. For the Os–Cr complex, electrophiles will attack the metal–metal bond, but for the Os–W complex, they will attack the CO ligand. On the other hand, the LUMO's of these complexes have the same character, which is antibonding between the two metal atoms. These LUMO's also expand around all the CO ligands.

Figure 10 shows the HOMO's and LUMO's of the $(OC)_5M-M(CO)_5$ (M = Mn, Re) complexes. They are $\sigma$-type bonding

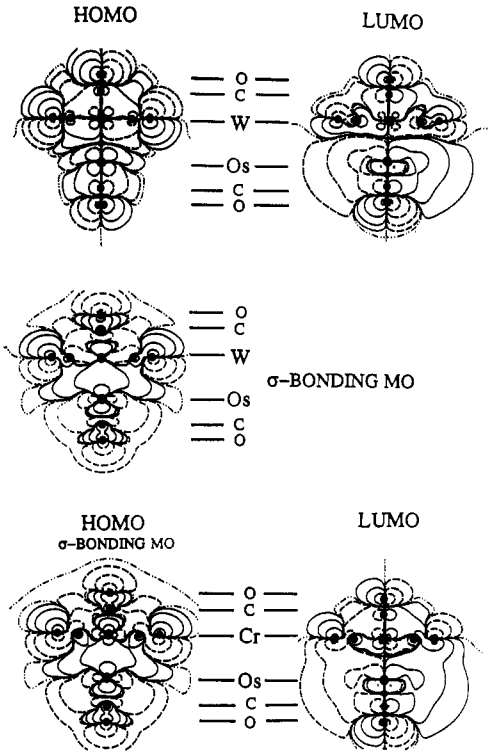


**Figure 9.** Contour maps of the HOMO and LUMO of $(OC)_5Os$–M-$(CO)_5$ (M = W, Cr). The highest occupied $\sigma$-orbital in $(OC)_5Os$–W-$(CO)_5$ is also drawn. The solid lines and the dashed lines indicate the plus and minus phases of the molecular orbitals.

and antibonding orbitals, respectively, between the two metal atoms.

## Conclusion

We have investigated the nature of the metal–metal bond in the $(OC)_5Os$–$M(CO)_5$ (M = W, Cr) complexes in comparison with the covalent metal–metal bond in the $(OC)_5M$–$M(CO)_5$ (M = Mn, Re) complexes. The results are summarized as follows.

(1) The metal–metal $\sigma$-bonds in $(OC)_5Os$–$M(CO)_5$ (M = W, Cr) are formed by a pair-electron transfer from the HOMO of $Os(CO)_5$ to the LUMO of $M(CO)_5$ (M = W, Cr). There are no back-donating orbitals. These metal–metal bonds are obviously dative bonds, as suggested experimentally.

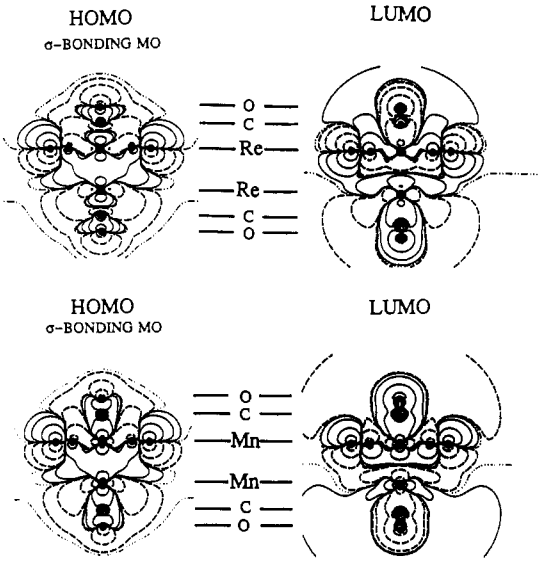


**Figure 10.** Contour maps of the HOMO and LUMO of $(OC)_5M$–M-$(CO)_5$ (M = Mn, Re). The solid lines and the dashed lines indicate the plus and minus phases of the molecular orbitals.

(2) The conformations, the equilibrium metal–metal distances, and the vibrational force constants of these complexes are well reproduced by the present calculations. The dative metal–metal bond could be described quantitatively, as well as the covalent metal–metal bond, in the framework of the present calculations.

(3) The dative metal–metal bonds in $(OC)_5Os$–$M(CO)_5$ (M = W, Cr) are less stable than the covalent metal–metal bonds in $(OC)_5M$–$M(CO)_5$ (M = Re, Mn), although the force constants are comparable with each other. This is because the geometry of the $Os(CO)_5$ fragment relaxes into the trigonal-bipyramid form at the dissociation limit and a large relaxation energy is obtained.

(4) When the dative metal–metal bond is formed, the electron transfer is not restricted to the metal–metal region, but occurs from the whole of $Os(CO)_5$ to the whole of $M(CO)_5$ (M = W, Cr) including all the radial CO ligands.

(5) The bonding in $(OC)_5Os$–$Cr(CO)_5$ is less stable than that in $(OC)_5Os$–$W(CO)_5$.

(6) The HOMO of the Os–Cr complex is a metal–metal $\sigma$-bonding orbital, while the HOMO of the Os–W complex is a metal–CO bonding orbital. Therefore, these complexes should have different reactivities to electrophiles.